Pathol. Oncol. Res. (2011) 17:315–324
DOI 10.1007/s12253-010-9319-x

RESEARCH

Open MR-Guided High-Dose-Rate (HDR) Prostate Brachytherapy: Feasibility and Initial Experiences Open MR-Guided High-Dose-Rate (HDR) Prostate Brachytherapy

Ferenc Lakosi · Gergely Antal · Csaba Vandulek · Arpad Kovacs · Gabor L. Toller · Istvan Rakasz · Gabor Bajzik · Janaki Hadjiev · Peter Bogner · Imre Repa

Received: 25 January 2010 / Accepted: 6 October 2010 / Published online: 11 January 2011

Abstract The aim of our pilot study was to demonstrate the feasibility and dosimetric quality of MR-guided HDR prostate brachytherapy in a low-field 0.35T open MRI scanner and to present our initial clinical experiences. 16 patiets with intermediate- to high-risk localized prostate cancer were treated with 46–60 Gy of external beam radiotherapy preceded and/or followed by an 8 Gy MR-guided HDR boost. For interventions an MR compatible custom-made system, coaxial needles and plastic catheters were used. Template reconstruction, trajectory planning, image guidance, contouring and treatment planning were exclusively based on MR images. For treatment planning, dose-point- and anatomy-based inverse planning optimization was used. Image quality was found to be good to excellent in almost all cases. The mean catheter placement accuracy modeled by Rayleigh distribution was 2.9 mm with a sigma value of 2.3 mm. The mean and standard deviation (SD) of the dosimetric results for the target volume were the following: V100: 94.2±4.3%, V150: 43.9±6.8%, V200: 18.5±5.9%. The mean $D_{0.1}$, D_1 and D1 values for the intraprostatic urethra were 117.6±12.5%, 98.5±19.9% and 122.3±16.4%, respectively. Regarding the rectal wall the mean $D_{0.1}$, D_1 and D_2 values were 77.3±7.2%, 64.8±7.5%, and 53.2±9.1%, respectively. The mean maximum dose for the inner rectal surface was 53.5±9.2%. No RTOG Grade 3 or worse acute toxicities were observed. Our method seems to be a promising approach for performing feasible, accurate and high-quality MR-guided HDR prostate brachytherapy. To determine the long term side effects and outcome higher number of patients, additional follow-up is needed.

Keywords HDR · Brachytherapy · Image guidance · Open MRI · Prostate cancer

Abbreviations

BT	Brachytherapy
BW	Pixel bandwidth
COIN	Conformality index
CTV	Clinical target volume
D_u1	Dose to volume of the most exposed 1% of the urethra
D90	Minimum dose with which 90% of the PTV was irradiated
DHI	Dose Homogeneity Index
D_{rmax}	Maximal point dose of the rectal inner surface
DNR	Dose Nonuniformity Ratio
$D_{r0.1}$ D_{r1}, D_{r2}	Dose to volume of the most exposed 0.1, 1 and 2 cm^3 of the rectal wall
$D_{u0.1}$,D_{u1}	Dose to volume of the most exposed 0.1 and 1 $cm^3$of the urethra
EBRT	External-beam radiotherapy
FA	Flip angle
FOV	Field of view
FSPGR	Fast spoiled gradient-echo
Gy	Gray

F. Lakosi · G. Antal · C. Vandulek · A. Kovacs (✉) · G. L. Toller · G. Bajzik · J. Hadjiev · P. Bogner · I. Repa
Health Center, University of Kaposvar,
Guba Sandor Street 40,
Kaposvar 7400, Hungary
e-mail: kovacs.arpad@sic.hu

I. Rakasz
Department of Urology, Kaposi Mor Teaching Hospital,
Tallian Gyula Street 20-32,
Kaposvar 7400, Hungary

HDR	High-dose-rate
HRPC	High-risk prostate cancer
IPO	Inverse planning optimization
IRPC	Intermediate-risk prostate cancer
MRI	Magnetic resonance imaging
NEX	Number of excitations
OARs	Organs at risk
Prs	Procedures
Pts	Patients
SV	Seminal vesicles
T	Tesla
T1W	T1-weighted
T2W	T2-weighted
TE	Echo-time
TR	Repetition time
TRUS	Transrectal ultrasound
V100,V150, V200	The volume in the PTV receiving 100% 150% or 200% of the prescribed dose or greater

Introduction

Prostate cancer is the most common male malignant tumor in the Western world. In Hungary, between 2001 and 2005 both the incidence and mortality show a slight decrease. However, prostate cancer remains the fourth most common male cancer holding a similar rank in terms of mortality [1].

Existing evidences show that biochemical control rates are improved if the delivered dose to the prostate gland is increased [2]. Besides modern external-beam radiotherapy (EBRT) techniques like 3D conformal radiotherapy or intensity-modulated radiotherapy, brachytherapy (BT) could be a feasible method for achieving local dose escalation with stable or reduced acute and late morbidity [3–5].

The gold standard technique for guidance of prostate biopsy and brachytherapy is transrectal ultrasound (TRUS) due to the ease of use, low costs and fast real-time 3D image acquisition connected with its new developments [6, 7]. The excellent soft tissue contrast and high sensitivity achieved by magnetic resonance imaging (MRI) was the main rationale for the introduction of MRI data into the prostate interventions [6, 8]. Furthermore, biologic-metabolic MRI imaging methods like spectroscopy, dynamic contrast-enhanced studies, and diffusion-weighted images are able to visualize the intraprostatic lesion, which makes targeted interventions, partial radiation dose delivery and dose painting possible [9–11]. The utility and clinical efficacy of MR-guided prostate BT has been demonstrated by an increasing number of groups [12–19].

Considering MR-guided prostate BT, three general approaches are actively under investigation, including diagnostic MR image fusion with the intraoperative ultrasound images [9], the use of low-field “open” MRI scanners (0.2–0.5 Tesla (T)) [12–15] and the direct use of high-field closed bore MRI systems (1.5–3T) [16–19]. Compared with high-field MRI systems, open scanners offer improved and convenient access to the patient during the procedure, although the image quality is poorer due to the low signal noise ratio available with lower magnetic field strength. However, several limiting factors exist, which prevent the routine use of closed-bore magnets for interventions. Primarily the complex and challenging environment inherent to MRI technology and constrained ergonomics of closed bore scanners make the regular, i.e. daily or weekly, access for these time consuming procedures difficult. On the other hand there are technical challenges like patient dimensions, -positioning, with the difficulty of perineal access, demanding the use of computer integrated robotic navigation and/or short, wide-bore MRI [18, 19].

In our Institution an open configuration MRI scanner is available for oncoradiology interventions with a capacity of four working days per week [20]. In the frame of our MR-guided prostate intervention program we have initiated a three phases -gel phantom, cadaver and healthy canine-study to develop a methodology for MR-guided high-dose-rate (HDR) prostate BT focusing on image quality [21]. The excellent preliminary results facilitated us to introduce this method into the clinical practice. In an attempt to answer the question whether open MRI unit is valuable tool for prostate HDR BT, we present a report of our methodology, image quality, needle placement accuracy, dosimetric results, acute morbidity and working time analysis.

Methods and Materials

Patient Cohort

Patients with intermediate- to high-risk prostate cancer (IRPC, HRPC) were eligible for study enrollment. Risk group definition was based on the recommendation of the National Comprehensive Cancer Network, Version 2, 2008 [22]. Staging examinations included initial prostate specific antigen measurement, digital rectal examination, histopathology review, 1.5T prostate MRI with pelvic phased coil and bone scan in HRPC. Exclusion criteria included contraindication for epidural anesthesia or MRI, previous transurethral resection of the prostate (TURP) within 6 months, large TURP defect, or high (>18) International Prostate Symptom Score or maximum uroflow rate <10 ml/s or

prostate volume >60 cm^3 or presence of pubic arch interference. The prospective study protocol was approved by the national ethical committee (record number: 84-261/2008-1018EKU).

Patient and Tumor Characteristics

Characteristics of patients and tumors are given in Table 1. Between January 2008 and May 2009 altogether 20 MR-guided prostate brachytherapy procedures have been successfully performed. 12 patients were treated with a single fraction of 8 Gy preceded or followed by EBRT. The remaining 4 patients received two implant sessions interposing EBRT. Three patients had visible extraprostatic tumor extension on MRI. All patients received neoadjuvant and concurrent hormonal therapy followed by adjuvant treatment in case of HRPC.

Positioning, Device Description

For guidance purposes of the BT, an "open" architecture 0.35T MRI scanner (Signa Ovation; General Electric Healthcare; Milwaukee; USA) was used. Due to the horizontally split open magnet design the interventions were performed with the patients placed in the right lateral decubitus position. The setup for the procedure is demonstrated in Fig. 1a,b. Details of the positioning, device description and template reconstruction have been previously described in a developmental canine study [21]. In brief, for the interventional procedures, an MR compatible device was designed consisting of a template-obturator rod (TOR) (Fig. 1c), an immobilization arm and patient tray (Fig. 1b). The patient tray was designed with an adjustable thermoplastic mask fixation mechanism, knee-leg holder stages and support cushions with tapes and bands which allow comfortable patient immobilization and transport. For imaging the manufacturer's general purpose 9 inch diameter surface coil was used, which was positioned at the patients gluteal region around the TOR (Fig. 1a,b). Template reconstruction was based on the filling of the template holes with sterile surgical gel, (Instillagel; Farco-Pharma Gmbh; Cologne; Germany), which allowed an excellent visualization of the template grid on the T2-weighted (T2W) fast spin-echo (FSE) images (Figs. 2a,c,d and 3) and smooth catheter insertion. Using our treatment planning systems (Theraplan Plus version 3.8; Anatomy Modelling; MDS Nordion; Quebec; Canada, Brachyvision version 8.1; Varian Medical Systems, Inc; Palo Alto; USA), the template grid was defined as a standard triangle grid-geometry punch pattern with a polygon-contour, so-called template-obturator contour (TOC). For image guidance and target confirmation, a T1-weighted (T1W) fast spoiled gradient-echo (FSPGR) sequence (Fig. 2b) (repetition time (TR): 100 ms, echo-time (TE) min, flip angle (FA) 60°, pixel bandwidth (BW) 10.42 Hz, field of view (FOV) 32 cm, slice thickness/spacing 5/0 mm, 256×192, 6 slices, Number of Excitations (NEX) 6, scan time:48 s) was used. For template reconstruction, trajectory planning, target delineation and treatment planning, T2W images (TR 3100 ms, TE 86 ms, FA 56°, BW 13.89 Hz, FOV 32 cm, slice thickness/spacing 5/0 mm, 256×192, 15–30 slices, NEX 4, scan time 3:56 min-7:36 min) were used.

Table 1 Patient and tumor characteristics

Variables	Values
Number of patients	16
Number of insertions	20
Age, years, mean (range)	67 (53–77)
Gland size, cm^3 (range)[a]	23.2 (15.6–32.7)
Intermediate-risk group	11
High-risk group	5
T stage[b]	
T1c	6
T2	7
T3a	3
iPSA, ng/ml, mean (range)	15.2 (3.9–24)
Gleason Score, mean (range)	5.4 (3–8)
IPPS, mean (range)	6.2 (1–18)
Qmax, mean (range)	16 (11–20.2)

iPSA initial prostate-specific antigen; *IPPS* International Prostate Symptom Score; Q_{max} maximum uroflow rate

[a] Pelvic MRI determined volume using the ellipsoid formula (0.52 × height × length × width)

[b] Based on clinical (American Joint Committee on Cancer Staging System, 6th edition) and pelvic MRI stage

Catheter Placement

Our application technique has been described in detail [20]. All patients underwent bowel preparatory regimen 1 day before the BT. Prophylactic antibiotics and α-blockers were used for 2 days (Ciprofloxacin 1 g/day, Tamsulosin 0.4 mg/day) preoperatively and then 1 week postoperatively. All procedures were performed under epidural anesthesia. A urinary bladder catheter filled with contrast agent (Omnipaque 350; General Electric Healthcare; Amersham; UK) was inserted into the bladder and clamped. After the patients were immobilized on the tray in the right lateral decubitus position and the perineum was sterilized, the obturator was inserted into the rectum and at the same time the jelly filled template was positioned firmly against the perineum. The TOR was then secured to the positioning stage which was already fixed on the patient tray. The coil was positioned and also fixed onto the tray. Imaging started with a 3D localizer followed by T2W FSE and T1W FSPGR sequences in all three planes. The axial slices were then digitally forwarded to the planning

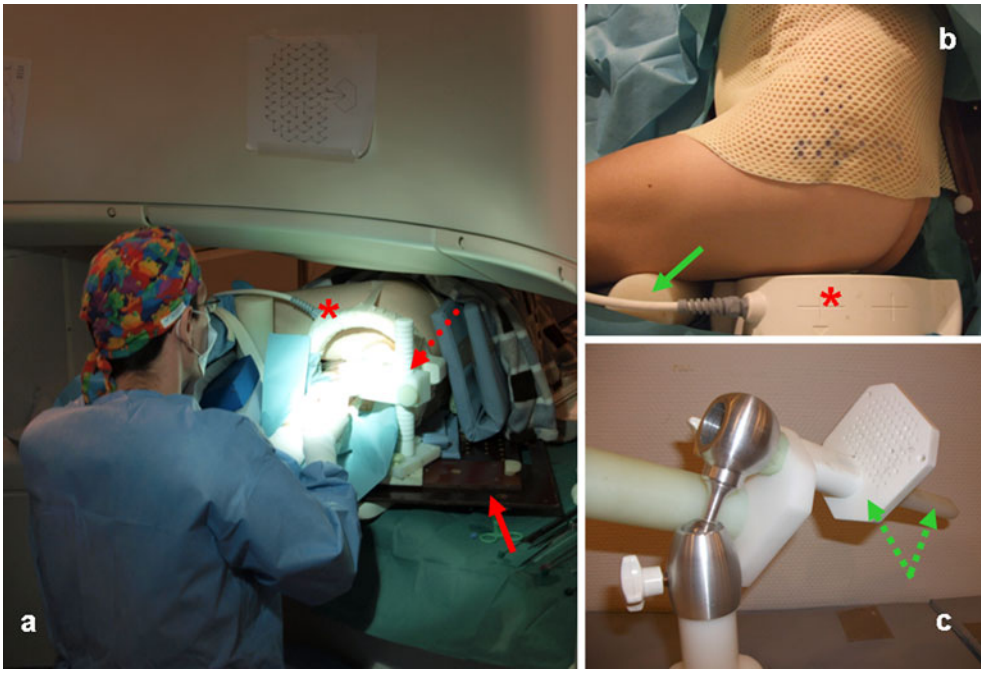

Fig. 1 (**a**) Patient set up in the open magnet during intervention. Note the feet-first right lateral decubitus position with maximized perineal access. Patient tray (*solid arrow*) also holds custom made device (*dotted arrow*), and the surface coil (*asterisk*). (**b**) Thermoplastic mask fixation mechanism along with knee holder stage (*green solid arrow*) stabilizes the patient. Note the surface coil (*asterisk*) at the gluteal region. (**c**) Custom made device, including template-obturator rod (*green dotted arrow*)

system. This was followed by template reconstruction and trajectory planning. The needles used for catheter placement were 14 G MRI compatible coaxial needles (In vivo Germany GmbH; Schwerin; Germany). For needle insertions, the scanner table was withdrawn from the magnet bore, and then advanced back to the isocenter for target confirmation. The locations of the needles were checked using axial and coronal FSPGR images. The accuracy of the needle tip artifacts was

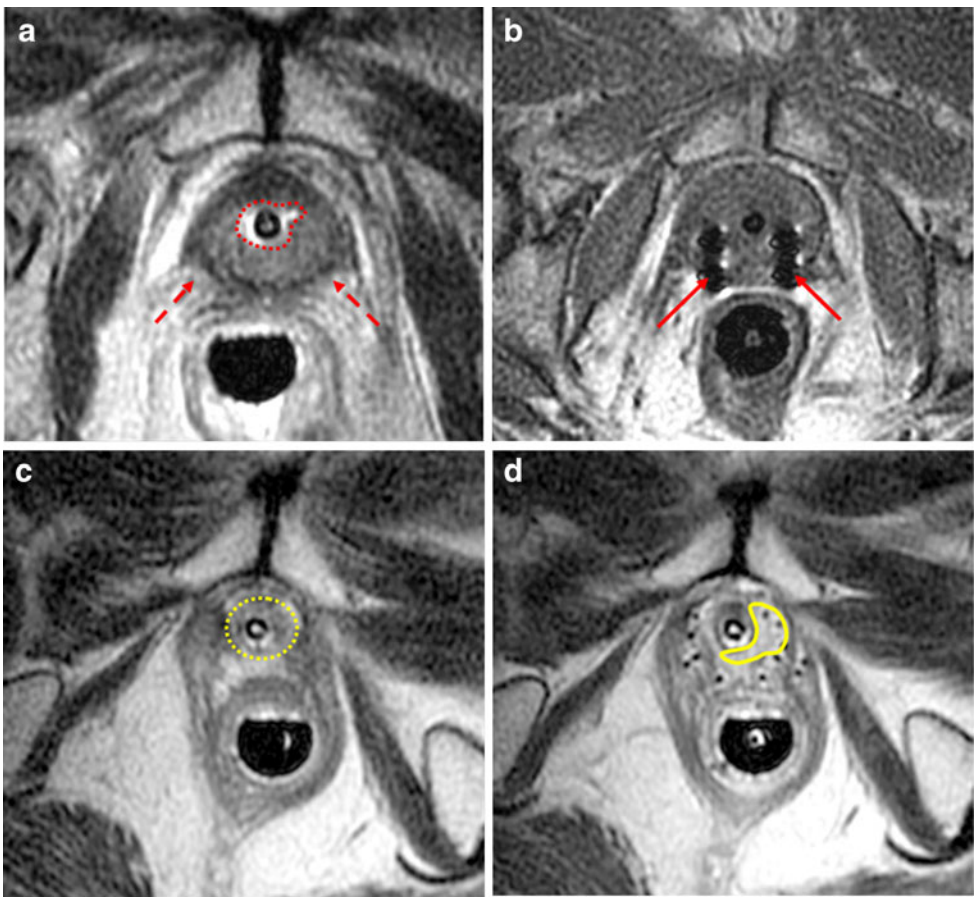

Fig. 2 Image quality. (**a**) T2W axial FSE slice at the mid-plane of the prostate. Note the transurethral resection cavity (*red dotted line*) clearly delineated by the high signal intensity urine surrounding the Foley catheter. Simultaneously, neurovascular bundles are well visualized (*dotted arrows*). (**b**) Axial view of T1W FSPGR images with the inserted coaxial needles (*solid arrows*). Corresponding pre-implant (**c**) and post-implant (**d**) T2W axial FSE images at the apical region. Apex (*yellow dotted line)* is well defined on picture "c". However, on picture "d" the apical contour is blurred on the right side (*solid line*) due to the high signal intensity edema and bleeding in the surrounding tissues

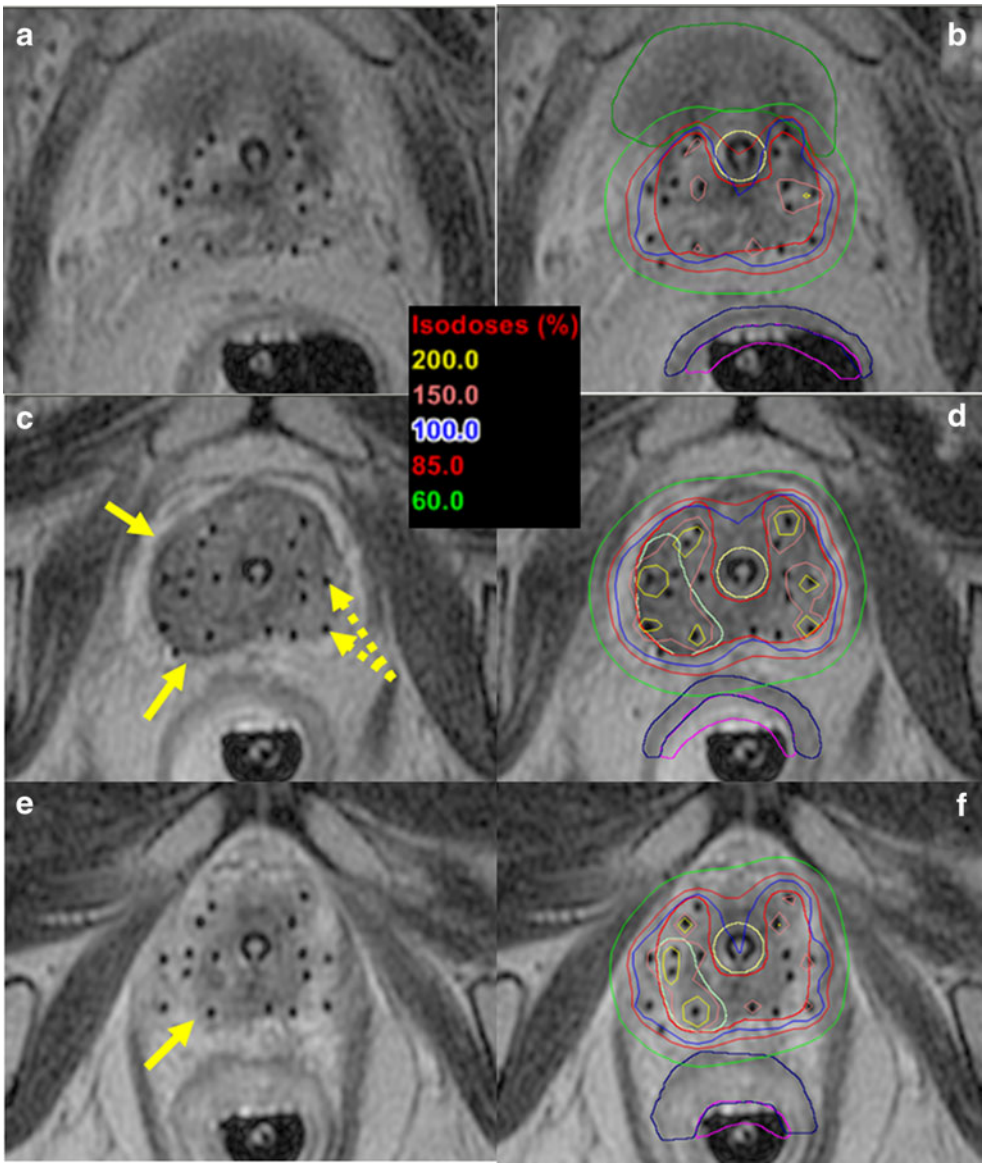

Fig. 3 Individualized dose distribution with simultaneous integrated boost. Representative MR slices at the base-, mid- and apical plane showing anatomy (**a**,**c**,**e**) with structures and isodose lines (**b**,**d**,**f**) in patient with cT3a prostate cancer. Note the posterolaterally bulging tumor on the right side involving the apical region also (*solid arrows* on **c**,**e**). Plastic catheters are clearly defined as small black dots (*dotted arrows*) without compromising target definition. Clinical target volume (*red*) and intraprostatic lesion (*light green*) covered by 100% (*dark blue*) and 150% (*pink*) isodose lines

confirmed by the re-projection of the TOC and when necessary, needle repositioning was undertaken. Once the physicians were satisfied with the position of the needles, the inner mandrin was removed and a plastic BT catheter (5 F; Proguide; 240 mm; Nucletron; Veenendaal; The Netherlands) was inserted through the coaxial needle. The outer part of the coaxial needle was then removed. The first 4–5 needles advanced primarily to the base plane, acting as fixation and reference needles. The subsequent needles and catheters were sequentially placed and advanced to the reference depth. On the control scans the template, prostate and patient shifts were also checked and when necessary, re-registration and/or trajectory modification were also made. Once all plastic catheters were inserted and fixed within the template, a final set of T2W FSE images with 3–5 mm slice thickness were acquired and loaded into the treatment planning workstation.

During transportation to the BT unit the patients were left in the immobilized, decubitus position on the tray and the TOR remained inserted into the rectum. The verification of the catheter position was based on the following: patient's tattoo displacements in relation to the mask holes, ink displacements on the catheters in relation to the TOR, measuring and recording of outer catheter lengths and finally a lateral X-ray image control (Siremobil Compact, Siemens; Erlangen; Germany). On this latter, the position of the catheters tip was subjectively verified in relation to the Foley balloon, rectal dosimeter and symphisis and compared with a corresponding sagittal MR image. In vivo rectal dosimetry (T9112 Five-fold semiconductor rectum probe, PTW-Freiburg) has been perfomed in all patients.

For radiation delivery, a HDR afterloading system (Gammamed plus, Varian, USA,) with ^{192}Ir stepping source was used.

Treatment Planning

Prostate periphery without margin was defined as the clinical target volume (CTV), which means the whole organ excluding the urethra and pre-urethral region (Fig. 3b,d,f). CTV also contains extraprostatic disease if present (Fig. 3c,d,e). Anterior rectal wall, anterior inner rectal surface and urethra with intraprostatic- and bulbo-membranousos part were delineated as organs at risk (OARs) (Fig. 3). In the present patient cohort bladder and neurovascular bundles (NVBs) were not systematically defined. In the first 6 procedures, only dose-point optimization (DPO) (Theraplan Plus version 3.8; Anatomy Modelling; MDS Nordion; Quebec; Canada) was used, while in the remaining 14 interventions, anatomy-based inverse planning optimization (IPO) was performed (Brachyvision version 8.1; Varian Medical Systems, Inc; Palo Alto; USA). The IPO planning system defines a cost function for each constraint, then sum all these cost functions weighted by the priority assigned, generating a Lagrange function, then searches for the local minima of this function using the downhill simplex algorithm. Dose constraints are presented in Table 2. The fraction dose of BT was 8 Gray (Gy). Depending on the delivered dose of 46 Gy or 60 Gy of EBRT this represents a normalized total dose in 2-Gy fractions (α/β ratio = 2 Gy) of 80–86 Gy, respectively. Besides the values given in Table 2 for dosimetric reporting D_u1, D_{r2} [23], Conformality index (COIN) [24], Dose Homogeneity Index (DHI) [25] and Dose Nonuniformity Ratio (DNR) [26] were calculated.

Table 2 Dose constraints

Structures	Values (%)
Target volume	
V100	>90
V150	≤40
V200	≤20
D90	≥95
Intraprostatic urethra	
$D_{u0.1}$	≤150
D_{u1}	≤125
Bulbo-membranousos urethra	
$D_{0.1}$	≤125
Rectal wall	
$D_{r0.1}$	≤85
D_{r1}	≤75
Rectal inner surface	
D_{rmax}	≤60

V100,150,200 the volume in the PTV receiving 100%,150% or 200%, of the prescribed dose or greater; *D90* the minimum dose with which 90% of the PTV was irradiated; $Du_{0.1}$,Du_1 dose to volume of the most exposed 0.1 and 1 cm^3 of the urethra; *Du1* dose to volume of the most exposed 1% of the urethra; $D_{r0.1}$, D_{r1}, D_{r2} dose to volume of the most exposed 0.1, 1 and 2 cm^3 of the rectal wall; D_{rmax} maximal point dose of the rectal inner surface

EBRT and Follow-Up

Patients received a total dose of 46–60 Gy of 3D conformal radiotherapy. In case of HRPC patients, the CTV1 included the pelvic lymph nodes with the prostate and seminal vesicles (SV) receiving up to 46 Gy with 2 Gy per fraction followed by 14 Gy boost to the prostate with 2 cm of the seminal vesicles (CTV2). For IRPC patients, the CTV1 included the prostate and SV, while the CTV2 covered the prostate with 1 cm of the SV. Planning target volume was created with an isotropic 1 cm margin around the CTV. Patients were seen by a radiation oncologist weekly during RT. The follow up schedule included 1–3 months visit for the first 2 years and annually thereafter. Acute toxicity was graded according to The Radiaton Therapy Oncology Group scale [27].

Statistical Analysis

For statistical evaluation the StatSoft Statistica 7.0 software was used. Since there were a very limited number of procedures in the DPO group, and we have switched to IPO relatively early, we have only given a descriptive statistical analysis about the DPO group. However, we compared the dosimetric values of the first 7 and last 7 procedures within the IPO cohort for the demonstration our learning curve. Differences in these values were assessed by a Wilcoxon Matched Pairs test analysis. A p value <0.05 was considered significant.

Results

Needle Placement Accuracy

The average number of inserted catheters was 13 (range: 11–17). We analyzed the accuracy of the first 100 plastic catheter placements. The maximum catheter deviation was measured as being the magnitude of the disagreement between the placed position and the intended target site (i.e. the projection of the virtual template hole) at the level of the plastic catheter's tip. The catheter placement accuracy was modeled by the Rayleigh distribution with a sigma value of 2.3 mm. The calculated mean and median catheter placement error was 2.9 mm and 2.7 mm, ranging from 0.0 mm to 5.0 mm. 91% of the errors were less than 4.0 mm.

Image Quality

Image quality was assessed by a consensus of two experienced readers including one radiologist and one radiation oncologist (BG,LF) using a four point scoring scale (1: excellent, 2: fair, 3: diagnosis or accuracy in doubt due to poor quality, 4: inadequate quality) on each pre- and post implant T2W images. The basis of the analysis was the following: visibility of the prostate at the base plane, mid-plane and apex; visibility of OARs; and visibility of the coaxial needle artifacts and plastic catheters. Image quality scores in percentage of the total number of collected pre- or postimplant series are demonstrated in Table 3.

Intervention Tolerance, Acute Morbidity

There were no intervention related urethral or rectal injuries. No infections, fever or neuropathy were observed. One patient experienced pressure injury to cutaneous pressure point on the right thigh due to inadequate support. All patients voided spontaneously shortly after the removal of the urinary catheter. Three of the 16 patients presented hematuria which resolved within 48 h in all cases. Perineal haematoma was noted in 2 patients with a resolution of 1 week. The hospitalization time was 3 days for all patients. During the combined therapy none of the patients developed Grade 3 or worse acute toxicity. The main acute genitourinary (GU) toxicities were dysuria, an increase in the frequency of urination or nocturia. The distribution of the acute GU toxicity grades in the patients (pts), overall, was as follows: Grade 0: 3 pts (19%), Grade 1: 5 pts (31%) and Grade 2 in 8 pts (50%). The main acute gastrointestinal (GI) toxicity was the increased bowel frequency. The pattern was as follows: Grade 0: 7 pts (44%), Grade 1: 5 pts (31%) and Grade 2 in 4 pts (25%).

Dosimetric Results

The dosimetric results are presented in Tables 4 and 5. The average V100, for all patients was: 94.2±4.3%. The average V100, V150 and V200 for DPO and IPO were 89.0±4.0 vs. 96.5±2.0, 42.2±6.6% vs. 44.6±6.9% and 22.8±7.9% vs. 16.7±3.7%, respectively. The average DHI, DNR and COIN were 52.5±9.5% vs. 52.8±6.9%, 39.7±6.7% vs. 33.7±4.7% and 69.2±7.0 vs. 67.6±5.9 for DPO and IPO, respectively. We compared the dosimetric values yielded in the first ($IPO_{1–7}$) and second half ($IPO_{8–14}$) of the procedures generated by IPO. We have noted superior results in all evaluated parameters in favor of the $IPO_{8–14}$ group. The difference was significant for the values of V150 (46.6% vs. 42.6%), DHI (49.4 vs. 56.3%) and DNR (35.1% vs. 32.3%) The improvement in value of V200 (17.6% vs. 15.7%) tended to reach the significant level (p=0.053). The average V100, D90 and COIN values were slightly better in the $IPO_{8–14}$ group, but the difference was not statistically significant (p=0.078–0.363). There were no significant change in the value of $D_{0.1}$ for bulbo-membranousos urethra (p=0.211), however all of the other parameters including intraprostatic urethra ($D_{u0.1}$: 127.1% vs. 114.2% D_{u1}: 111.3% vs. 103.6%, D_u1: 136.4% vs. 119.1%), rectal wall ($D_{r0.1}$: 77.3% vs. 74.1%, D_{r1}: 68.6% vs. 59.5%, D_{r2}: 60.9% vs. 53.0%) and rectal inner surface (D_{rmax}: 58.8% vs. 50.8%) were significantly lower in the $IPO_{8–14}$ group, respectively.

Overall Procedure Time

The duration of the procedures for all patients from the beginning of patient positioning to the removal of the catheters, ranged between 4.5 and 8.5 h, with a mean of 5.7 h. The procedure time for the first two patients was 8.5

Table 3 Image quality assessment

Structures	Pre-implant%				Post-implant%			
Image quality score	1	2	3	4	1	2	3	4
Prostate								
base plane	95	5	0	0	90	10	0	0
midplane	100	0	0	0	100	0	0	0
apex	65	35	0	0	45	40	15	0
OARs								
rectal wall[a]	95	5	0	0	95	5	0	0
rectal inner surface[a]	100	0	0	0	100	0	0	0
intraprostatic urethra[b]	100	0	0	0	100	0	0	0
bulbo- membranousos urethra[b]	100	0	0	0	100	0	0	0
NVBs	60	40	0	0	45	30	25	0
Coaxial needles	–	–	–	–	100	0	0	0
Plastic catheter	–	–	–	–	100	0	0	0

OARs organs at risk; *NVBs* neurovascular bundles

[a] with obturator

[b] with Foley catheter

Table 4 Dosimetric results for the target volume

Parameters (%)	Mean±SD					*p* values
	All prs	DPO	$IPO_{1–14}$	$IPO_{1–7}$	$IPO_{8–14}$	$IPO_{1–7}$ vs. $IPO_{8–14}$
V100	94.2±4.3	89.0±4.0	96.5±2.0	96.0±2.0	97.0±1.0	0.0782
V150	43.9±6.8	42.2±6.6	44.6±6.9	46.6±9.4	42.6±6.8	0.0198
V200	18.5±5.9	22.8±7.9	16.7±3.7	17.6±5.0	15.7±1.7	0.0535
D90	105.0±7.9	99.1±5.1	107.5±7.7	106.7±7.7	108.4±8.2	0.3630
DHI	52.8±6.9	52.5±9.5	52.8±6.9	49.4±8.1	56.3±3.1	0.0089
DNR	35.5±5.9	39.7±6.7	33.7±4.7	35.1±5.6	32.3±3.5	0.0075
COIN	68.4±8.5	69.2±7.0	67.6±5.9	67.0±4.3	68.1±7.5	0.3066

prs procedures; *SD* standard deviation; *V100,150,200* the volume in the PTV receiving 100%,150% or 200%, of the prescribed dose or greater; *D90* the minimum dose with which 90% of the PTV was irradiated; *COIN* Conformality index; *DHI* Dose Homogeneity Index; *DNR* Dose Nonuniformity Ratio

and 7.5 h, which showed a reduction to 4.5–6.5 h in the following procedures.

Discussion

To date only a few experiences have been published on MR-guided prostate BT, especially in the field of HDR BT [12, 13, 15–17]. Open configuration MRI scanners have already been successfully introduced into prostate biopsy, permanent seed implantation, furthermore, in many centers it has become the routine imaging modality for cervical cancer HDR BT [12, 13, 20, 28, 29]. Limitations inherent to low-field systems such as lower image quality and the inability of direct integration of biologic image information facilitated some centers to move toward high-field closed-bore MRI scanners [16–19]. Although the preliminary results are promising the routine clinical use is still pending.

Our goal was to introduce a prostate MR-guided HDR BT method which provides good image quality and fits into the frame of our daily clinical routine. Recently Ares et al. published a similar pilot study with hypofractionated HDR boost in an open MRI unit [15]. They reported an excellent 3-year biochemical control besides favorable acute and late side toxicities [15]. In our report we primarily focused on the technical feasibility, the dosimetric results and image quality.

We demonstrated in Table 3., that good image quality could be achieved with our low-field scanner. On pre-implant T2W FSE images prostate parenchyma, zonal anatomies as well as OARs are excellently visualized. Intraprostatic urethra with or without transurethral resection cavity (Fig. 2a,b), bulbo-membranousos urethra with distal urethral sphincter are easily differentiated, with the possibility of creating separated dose constraints on them. However, on post-implant T2W FSE images the clear delineation of the apex and the NVBs at this level could be

Table 5 Dosimetric results for the OARs

Parameters (%)	Mean±SD					*p* values
	All prs	DPO	$IPO_{1–14}$	$IPO_{1–7}$	$IPO_{8–14}$	$IPO_{1–7}$ vs. $IPO_{8–14}$
Intraprostatic urethra						
$D_{u0.1}$	117.6±12.5	110.5±6.7	120.7±13.3	127.1±11.1	114.2±12.7	0.0014
D_{u1}	98.5±19.9	77.9±22.7	107.5±9.9	111.3±8.8	103.6±10.1	0.0021
D_u1	122.3±16.4	110.1±6.5	127.1±16.8	136.4±17.5	119.1±12.2	0.0045
Bulbo-membranousos urethra						
$D_{0.1}$	69.9±13.9	68±17.4	71.8±14.9	71.2±13.3	69.4±15.2	0.2114
Rectal wall						
$D_{r0.1}$	77.3±7.2	73.2±4.3	83.3±8.1	77.3±7.2	74.1±8.1	0.0026
D_{r1}	64.8±7.5	66.8±5	64.1±8.2	68.6±5.6	59.5±8.1	0.0031
D_{r2}	53.2±9.1	44.4±8.3	56.9±6.4	60.9±6	53±6.8	0.0064
Rectal inner surface						
D_{rmax}	53.5±9.2	49.8±9.2	54.8±9.1	58.8±8.7	50.8±8.3	0.0058

OARs organs at risk, prs: procedures; *SD* standard deviation; $D_{u0.1}$, D_{u1} dose to volume of the most exposed 0.1 and 1 cm^3 of the urethra; D_u1: dose to volume of the most exposed 1% of the urethra; $D_{r0.1}$, D_{r1}, D_{r2} dose to volume of the most exposed 0.1, 1 and 2 cm^3 of the rectal wall; D_{rmax} maximal point dose of the rectal inner surface

difficult due to the implantation induced high-signal intensity intra-and/or periprostatic oedema and bleeding with similar findings in the surrounding muscles (Fig. 2c,d). These deficiencies could be solved by using multiplanar series, pre-implant images with or without image fusion.

Patients with detected intraprostatic lesion(s) with or without extracapsular extension on MRI may benefit from this procedure because individualized dose distribution could be generated including the high risk areas with the possibility of local dose escalation (Fig. 3) [10, 15, 16]. Additionally, on FSE sequences the plastic catheters are well and easily defined, no metallic artifacts are presented, further improving the validity of target definition (Fig. 3).

Few published experiences are available considering lateral decubitus position during MR-guided prostate interventions, especially in the field of BT [16, 17, 28]. The first experience came from Menard et al. [16] at 1.5T MRI scanner. In our case, the choice of this position was also due to the design of the magnet. However, compared to closed-bore systems, the architecture of our scanner allows us to achieve more extended and fixed leg elevation, which further improves the perineal exposure (Fig. 1a). Pubic arch interference has been observed in only two candidates with extremely narrow bony anatomy.

Our target coverage (mean V100: 94.2%) compared favorably with those published for HDR implants performed under MRI (mean V100: 83.4–92.9%) [15, 16, 30] or ultrasound guidance with or without inverse-planning (mean V100: 84.2–97.1%) [31–34]. Similarly to the results of other groups, our target coverage has markedly improved with the introduction of IPO (V100: DPO: 89% vs. IPO: 96.5%) [16]. The value of V150 (mean: 43.9%) seems to be a slightly higher when compared with the other published results (mean V150: DPO: 51.7%, Geometrical Optimization: 30.2–42.9%, IPO: 30.2–36.9%) [31, 32, 34]. This finding could be explained by the use of integrated boost in 5 procedures, the use of DPO in 6 procedures, the relatively low number of inserted catheters and the beginning of our learning curve. The improving dosimetric results within the IPO cohort well demonstrated our learning curve. The dose delivery of almost all OARs showed significant reduction besides the improved dosimetric values for the target volume (Tables 4 and 5).

The knowledge of needle placement accuracy is crucial during MRI-guided prostate interventions. The reported mean errors of coaxial needle placements during transperineal MR-guided biopsy [14, 17] ranged from 2.1 to 6.93 mm. In our previous canine study the average needle accuracy of 37 insertions experienced was 2.9 mm, with the maximum error of 4.5 mm [21]. In the human study we could adequately reproduce these results (mean: 2.9 mm, maximum error: 5 mm) with the exception that we chose to analyze the plastic catheter tip deviations, instead of metallic ones for three main reasons. First, treatment planning and consequently the quality of the BT absolutely depend on the reconstruction of the plastic catheters. Secondly, the coaxial needles we use do not always reach the base plane, thus additive catheter deviation could exist in the remaining tissue length. Third reason is the significantly lower artifact effect leading to more accurate results (Fig. 2b vs. Fig. 3). The large sample size may also confirm the relevancy of our results. Corresponding with the other author's findings through our registration method, it appeared that needle deflection was the main reason for these errors [14, 17]. These errors may be further reduced with the introduction of robotic systems [18, 19]. The preliminary results in the canine model in a high-field MRI scanner were excellent with a 2.02 (range, 0.86–3.18 mm) and 2.5 mm (range, 1.45–10.54 mm) median error for needle and seed placement [19].

The well known disadvantage of MR-guided procedures is the prolonged procedure time. Menard et al. [16] performed their first HDR brachytherapy session in 8.5 h on a 1.5T MR scanner. As they gained more experiences and used an inverse planning system with larger number of coaxial needles, the overall procedure time showed a marked reduction, but sill remained around 5 h. Our preliminary findings were similar with the note that the introduction of IPO along with the increasing experience has not brought significant improvement in the procedure time yet. Besides the challenging environment related to MRI technology, additional reasons may be the following: time consuming patient positioning, learning curve for IPO, higher number of defined structures, incorporation of the outer catheter length in the reconstruction of the first dwell time position and MRI modeling of the rectal dosimeter probe for the predictive estimation and verification of rectal wall dose delivery, which is the subject of our future work [35].

Conclusion

A system for transperineal MR-guided prostate BT has been developed and applied successfully on prostate cancer patients. Low-field MRI unit seems to provide a feasible, accurate, reliable image guidance and has become a part of our daily clinical practice. Higher number of patients and longer follow up are needed to determine the late side effects and outcome. Dose escalation, introduction of fractionated treatments and integration of high-field imaging in BT planning are planned in the near future.

Acknowledgements The authors thank Andras Bucsek for the development of the custom made system, Georgina Fröhlich for her help in the statistical analysis and the Urologic and Anesthesiologic team at the Kaposi Mor Teaching Hospital for their input and support.

References

1. Kásler M, Sz O (2008) European and Hungarian national tasks in oncology. Magy Onkol 52:21–33
2. Jereczek-Fossa BA, Orecchia R (2007) Evidence-based radiation oncology: definitive, adjuvant and salvage radiotherapy for non-metastatic prostate cancer. Radiother Oncol 84:197–215
3. Morton G (2005) The emerging role of high-dose-rate brachytherapy for prostate cancer. Clin Oncol 17:219–227
4. Hoskin PJ, Motohashi K, Bownes P et al (2007) High dose rate brachytherapy in combination with external beam radiotherapy in the radical treatment of prostate cancer: initial results of a randomised phase three trial. Radiother Oncol 84:114–120
5. Guix B, Bartina JM, Henriquez I et al (2007) Dose escalation by combined treatment 3-D conformal radiotherapy plus HDR brachytherapy as treatment for intermediate-or-high-risk cancer: early toxicity and biochemical outcome of a prospective randomized trial. [Abstract] Radiother Oncol 83(suppl1):82a
6. Presti JC Jr (2000) Prostate cancer: assessment of risk using digital rectal examination, tumor grade, prostate-specific antigen, and systematic biopsy. Radiol Clin North Am 38:49–58
7. Aigner F, Mitterberger M, Rehder P et al (2010) Status of transrectal ultrasound imaging of the prostate. J Endourol 24:685–691
8. Futterer J (2007) MR imaging in the local staging of prostate cancer. Eur J Radiol 63:328–334
9. Morgan VA, Kyriazi S, Ashley SE et al (2007) Evaluation of the potential of diffusion-weighted imaging in prostate cancer detection. Acta Radiol 48:695–703
10. Kim Y, Hsu IC, Lessard E et al (2008) Class solution in inverse planned HDR prostate brachytherapy for dose escalation of DIL defined by combined MRI/MRSI. Radiother Oncol 88:148–155
11. Van Lin EN, Futterer JJ, Heymink SW et al (2006) IMRT boost dose planning on dominant intraprostatic lesions: gold marker-based three-dimensional fusion of CT with dynamic contrast-enhanced and 1H-spectroscopic MRI. Int J Radiat Oncol Biol Phys 65:291–303
12. Tempany C, Straus S, Hata N et al (2008) MR-guided prostate interventions. J Magn Reson Imaging 27:356–367
13. Cormack RA, Kooy H, Tempany CM et al (2000) A clinical method for real-time dosimetric guidance of transperineal 125I prostate implants using interventional magnetic resonance imaging. Int J Radiat Oncol Biol Phys 46:207–214
14. Blumenfeld P, Hata N, DiMaio S et al (2007) Transperineal prostate biopsy under magnetic resonance image guidance: a needle placement accuracy study. J Magn Reson Imaging 26:688–694
15. Ares C, Popowski Y, Pampallona S et al (2009) Hypofractionated boost with high-dose-rate brachytherapy and open magnetic resonance imaging-guided implants for locally aggressive prostate cancer: a sequential dose-escalation pilot study. Int J Radiat Oncol Biol Phys 75:656–663
16. Menard C, Susil RC, Choyke P et al (2004) MRI-guided HDR prostate brachytherapy in standard 1.5T scanner. Int J Radiat Oncol Biol Phys 59:1414–1423
17. Susil RC, Camphausen K, Choyke P et al (2004) System for prostate brachytherapy and biopsy in a standard 1.5T MRI scanner. Magn Reson Med 52:683–687
18. Fischer GS, DiMaio SP, Iordachita II et al (2007) Robotic assistant for transperineal prostate interventions in 3T closed MRI. Med Image Comput Comput Assist Interv Int Conf Med Image Comput Comput Assist Interv 10:425–433
19. Muntener M, Patriciu A, Petrisor D et al (2008) Transperineal prostate intervention: robot for fully automated MR imaging–system description and proof of principle in a canine model. Radiology 247:543–549
20. Hadjiev J, Antal G, Antalffy Z et al (2004) A novel technique with a flexible applicator for MRI-based brachytherapy of cervical cancer. Eur J Gynaecol Oncol 25:347–350
21. Lakosi F, Antal G, Vandulek C et al (2009) Technical feasibility of transperineal MR-guided prostate interventions in a low-field open MRI unit: canine study. Pathol Oncol Res 15:315–322
22. National Comprehensive Cancer Network: National practice guidelines in oncology-prostate cancer, Version 2, 2008 (monograph online). http://www.nccn.org/professionals/physician-gls/PDF/prostate.pdf
23. Kovács G, Pötter R, Loch T, Hammer J et al (2005) GEC/ESTRO-EAU recommendations on temporary brachytherapy using stepping sources for localised prostate cancer. Radiother Oncol 74:137–148
24. Baltas D, Kolotas C, Geramani K et al (1998) A conformal index (COIN) to evaluate implant quality and dose specification in brachytherapy. Int J Radiat Oncol Biol Phys 40:515–524
25. Major T, Polgar C, Somogyi A et al (2000) Evaluation of the dose uniformity for double-plane high dose rate interstitial breast implants with the use of dose reference points and dose non-uniformity ratio. Radiother Oncol 54:213–220
26. Wu A, Ulin K, Sternick ES (1988) A dose homogeneity index for evaluating 192Ir interstitial breast implants. Med Phys 15:104–107
27. Cox JD, Stetz J, Pajak TF (1995) Toxicity criteria of the Radiation Therapy Oncology Group (RTOG) and the European Organization for Research and Treatment of Cancer (EORTC). Int J Radiat Oncol Biol Phys 31:1341–1346
28. Zangos S, Eichler K, Engelmann K et al (2005) MR-guided transgluteal biopsies with an open low-field system in patients with clinically suspected prostate cancer: technique and preliminary results. Eur Radiol 15:174–182
29. Potter R, Kirisits C, Fidarova EF et al (2008) Present status and future of high-precision image guided adaptive brachytherapy for cervix carcinoma. Acta Oncol 47:1325–1336
30. Citrin D, Ning H, Guion P et al (2005) Inverse treatment planning based on MRI for HDR prostate brachytherapy. Int J Radiat Oncol Biol Phys 61:1267–1275
31. Morton GC, Sankreacha R, Halina P et al (2008) A comparison of anatomy-based inverse planning with simulated annealing and graphical optimization for high-dose-rate prostate brachytherapy. Brachytherapy 7:12–16
32. Jacob D, Raben A, Sarkar A et al (2008) Anatomy-based inverse planning simulated annealing optimization in high-dose-rate prostate brachytherapy: significant dosimetric advantage over other optimization techniques. Int J Radiat Oncol Biol Phys 72:820–827
33. Akimoto T, Katoh H, Kitamoto Y et al (2006) Anatomy-based inverse optimization in high-dose-rate brachytherapy combined with hypofractionated external beam radiotherapy for localized prostate cancer: comparison of incidence of acute genitourinary toxicity between anatomy-based inverse optimization and geometric optimization. Int J Radiat Oncol Biol Phys 64:1360–1366
34. Fröhlich G, Agoston P, Lövey J et al (2007) Dosimetric evaluation of interstitial high-dose-rate implants for localised prostate cancer. Magy Onkol 51:31–38
35. Antal G, Lakosi F, Vandulek CS et al (2009) MR modelling of the rectal dosimeter probe during MR-guided high-dose-rate (HDR) prostate brachytherapy: feasibility and initial experiences. [Abstract] Radiother Oncol 91(1):38